Multifunctional colloidal-based nanoparticles for cancer treatment

Rita Falcão Baptista Ribeiro Mendes

Abstract

Cancer has one of the highest mortality rate worldwide. Nowadays therapies present high toxicity and secondary effects, low selectivity and pharmacokinetics' problems.

The presented propose aims to create a multifunctional lipid system containing the drug Doxorubicin (DOX) conjugated with graphene quantum dots (GQD) used as nanocarriers and photosensitive agents. This system will allow the selective and controlled release of DOX and will combine a therapeutic effect with imaging applications, being also stealthy to the immune system.

To achieve the proposed goals, two methods of GQD synthesis were developed: acid oxidation by Hummer's method (GQD-CB) followed by extrusion to obtain a size separation (GQD-CBext), and chemical vapour deposition (GQD-CVD). GQD were characterized by fluorescence, dynamic light scattering (DLS), confocal Raman spectroscopy, scanning electron microscopy (SEM) and infrared spectroscopy (ATR-FTIR).

DOX was studied by UV-VIS spectroscopy and ATR-FTIR and its ionization at different pH values was evaluated *in silico*.

In silico studies also allowed to evaluate the pH effect on the interaction between DOX and GQD-CB. Samples were characterized at pH 3, 6, 9 and 11 since these pH values represent the possible electrostatic interactions that can occur between GQD and DOX (no interaction; attraction; attraction and repulsion; repulsion, respectively). The electrostatic interaction and conjugates formation was confirmed by fluorescence, Raman, ATR-FTIR and UV-VIS spectroscopy.

GQD incorporation into lipid systems was studied by energy transfer (FRET) analysis between membrane probes and GQD.

Key Words: Graphene quantum dots (GQD), Doxorubicin (DOX), Liposomes, Nanocarriers for drug delivery, Cancer treatment

1. Introduction

Cancer is one of the most lethal pathologies and classical chemotherapy possesses high levels of cytotoxicity and low therapeutic efficiency [1]. Therefore, it is urgent to develop new therapies, more efficient and less toxic. In this regard, the main goal of the study described herein is developing multi-strategic lipid nanocarriers (LNC) that can simultaneously act as drug delivery systems and allow the drugs' pathway monitorization until it reaches the target cells in a controlled way [2].

The main components of the proposed LNC are: graphene quantum dots (GQDs) as nanovectors and photosensitive agents, doxorubicin as anti-cancer drug and liposomes as multifunctional lipid systems.

LNC are supposed to be multipurpose biocompatible systems that gather different strategies: (i) therapy, by drug delivery; (ii) imaging, by the optical properties of the nanocarriers (graphene quantum dots (GQDs)); (iii) triggering, by using pH-sensitive GQDs-drug conjugates; (iv) targeting, with passive or active strategies; and (v) stealth through polymeric coating of LNC. [2].

Carbon is one of the most abundant element on universe and human body and its chemical properties allow the formation of allotropes. Within carbon allotropes, graphene had gained the attention of the scientific world due to its mechanical, optical and electric properties.

There are several different methods to produce carbon dots, based on top-down (nano-cutting of carbon sources like rGO, GO, CNTs, fullerenes, graphite, among others) and bottom-up (based on dehydration and carbonization of carbohydrates from small molecules and polymers) approaches that give raise to different kinds of carbon dots, with different intrinsic characteristics and quantum yields (QY). From the available methods, acid oxidation and Chemical vapour deposition (CVD) were explored in an attempt to produce graphene dots.

Although the optical properties of CDs are dependent on a number of factors, there are some common aspects that must be referred. CDs all absorb in the UV region with a well-defined absorption band at 230 nm due to the π-π* transition of aromatic C=C bonds, and an absorption shoulder in the VIS region at about 300 nm that is related with the n-π* transition of the C=O bonds. Carbon dots have already been studied for some therapeutic applications as bioimaging, drug delivery systems, chemosensors, DNA cleavage.

The hydrochloride salt of doxorubicin (DOX) belongs to the anthracyclines family, a group of anti-carcinogenic drugs. Doxorubicin is composed by a quinone and hydroquinone tetracyclic ring (anthracyclinone) bonded to a daunosamine sugar. The presence of quinone and hydroquinone moieties on adjacent rings enhance the loss and gain of electrons and consequently the propensity of the molecule to react with iron to form free radicals. These radicals form reactive intermediates that disrupt nucleic acid bases, being this mechanism responsible for the antineoplastic activity and high toxicity [3] [4]. It is also important to mention the DOX dimerization that may occur for concentrations as low as 1 μM [5]. Dimerization is the process of self-aggregation that the drug suffer where the monomers aggregate to each other forming oligomers. It may occur at low and high concentrations.

DOX is used as anti-cancer drug on the majority of the cancer types nowadays and it has three mechanisms of action: (i) intercalation in DNA, (ii) inhibition of topoisomerase II, (iii) formation of reactive oxygen species (ROS). Its action may be compromised by the development of resistance and by the dimerization effect. Besides, as DOX acts in strongly proliferative cells it affects healthy cells and tissues with high proliferation (bone marrow, gonads, gastrointestinal tract).

The optical properties of the anthracyclines result from a complex interplay of several factors as the environment at which they are and the interactions with lipids, surfactants or membranes. However, their self-association into dimers above a critical concentration is one of the most relevant factors to take into account in optical analysis. [6] [7] [5]

The UV-VIS absorption spectrum of DOX has a broad main band with its centre at 490 nm and a shoulder at 360 nm [8] [9]. This shape is related with the permitted π-π* transition (1A -> 1Lb) polarized along the long axis and to the partially forbidden by electric dipole n- π* transition (1A -> 1La) of the three C=O groups, respectively [6] [10]. DOX absorption is strongly affected by the protonation state of the dihydroxyanthraquinone and almost unaffected by the protonation of the sugar that is not conjugated with the aromatic ring. DOX self-aggregation also affects its absorption [10]. Fluorescent behaviour of DOX is a much more complex mechanism. DOX fluorescence is wavelength dependent and the emission peaks alter in different ways with the type of solvent where DOX is solubilized, the pH of the solution and the concentration of DOX [5] [11] [12]. The two main characteristic peaks appear at 560 nm (I1) and 590 nm (I2), being possible to occur a third peak at 630 nm (I3) [10].

Liposomes are vesicles made of phospholipid bilayers that mimic the natural lipid environment of biological membranes. Since they are biodegradable and biocompatible and due to their tunable size and lipid polymorphism, liposomes have several advantages, such as: sustained release of drug, specificity achieved by targeting strategies like surface functionalization by target ligands, higher drug bioavailability, higher cellular adsorption, good encapsulation efficiency and ability to encapsulate greater amounts of drug.

GQD, DOX and conjugates of DOX and GQD were produced and characterized by: UV-VIS spectroscopy; fluorescence, with energy transfer (FRET) and quenching analysis; dynamic and electrophoretic light scattering (DLS and ELS), confocal Raman spectroscopy, attenuated total reflectance – Fourier transform infrared spectroscopy (ATR-FTIR) and scanning electron microscopy (SEM).

2. Experimental

2.1. Preparation and characterization of GDQ

Graphene quantum dots were prepared by acid oxidation through Hummer's method, from a CX-72 carbon black source (GQD-CB) and were used in suspensions randomly sized and separated by size by an extrusion method (GQD-CBext). Besides, GQD were also obtained by chemical vapour deposition (GQD-CVD) and extracted from glass substrate through a pH-sensitive and sonication method.

GQD-CB and GQD-CBext were characterized by fluorescence, ELS and DLS and UV-VIS absorbance at different pH values; whereas GQD-CVD were characterized by confocal Raman, SEM, DLS and ELS on glass substrate and pH 9 suspension.

2.2. Preparation and characterization of DOX solutions

Using the SMILES (Simplified Molecular Input-Input Line-Entry System) notation and the Chemaxon® software with the MarvinSketch® module, we proceeded to design the chemical structure of the DOX molecule to its three-dimensional representation and the *in silico* calculation of several chemical descriptors such as ionization, pKa, electrical characteristics and surface topology.

One stock aqueous solution and four DOX solutions were prepared at pH=0.9, 4.7, 9.4 and 11.9 with concentrations ~10^{-4} M. Six DOX standard solutions were obtained at each pH value and the molar extinction coefficients were calculated using UV-VIS spectroscopy.

2.3. Preparation and characterization of DOX-GQD conjugates

DOX and GQD interaction at different pH values was evaluated by *in silico* studies.

Four different working concentrations of DOX ($5x10^{-4}$, $6x10^{-4}$, $7x10^{-4}$, $8x10^{-4}$ M) were prepared in different pH buffers (pH 3, 6, 9 and 11) and used to prepare 16 conjugates (DOX-GQD-CB) with 1 mg of GQD-CB each. Conjugates were characterized by fluorescence, UV-VIS spectroscopy, Raman and ATR-FTIR.

2.4. Incorporation of GQD into liposomes

Liposomes and labelled liposomes were prepared as previously reported [87]. Briefly, a lipid film was prepared by evaporation to dryness of a mixture of ethanolic solutions of DMPC and a fluorescent probe (*n*-antroyloxy stearic acid derivatives where *n*=3 or 12, briefly designated as 3AS and 12AS). Lipid suspensions were then extruded under controlled temperature (37 ºC) through polycarbonate filters with a pore diameter of 100 nm to form large unilamellar vesicles (LUVs).

For each probe, a labelled liposomal sample was kept as reference and to 3 labelled liposomal samples were added: (i) GQD-CVD, (ii) GQD-CB and (iii) GQD-CBext. The labelled liposomes

were incubated with GQD at 37 ºC during 30 minutes in the dark. The incorporation of GQD into the liposomes was measured by fluorescence.

3. Results and discussion

3.1 GQD characterization

The π-π* (from C=C) and n-π* (from C=O) UV-VIS absorption peaks of GQD are presented in Figure 1 (left). The fluorescence excitation spectrum has shown pH dependency, presenting a maximum of 480 nm for pH<4.5 and 5<pH<11.5 and a second peak at 320 nm at pH 5 and 11.5 indicative of two species contributing to fluorescence (Figure 1 - right).

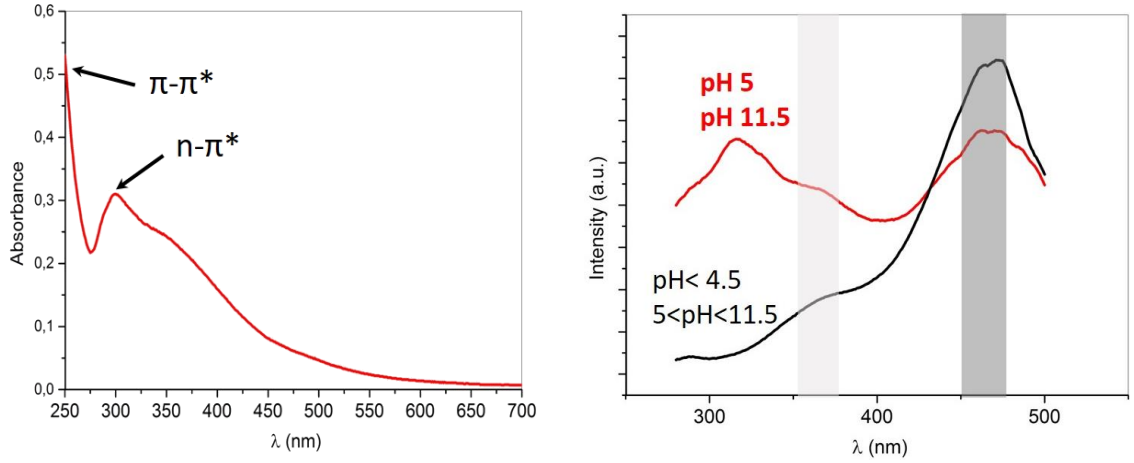

Figure 1 – Left: GQD-CB absorbance spectrum at pH=6. Right: Excitation spectra of GQD-CB at pH =5 and 11.5 (red line) and at pH<4.5 and 5<pH<11.5 (black line).

The emission spectra allowed to confirm that there is a co-existence of two fluorescent species at pH 5 and 11.5, since there is an isosbestic point in the spectra that is not visible in the other values of pH below 5 and between 5 and 11.5 (Figure 2 left). At pH 5 the isobestic point is associated with the dissociation of the carboxyl group, and at pH 11.5 with the dissociation of the hydroxyaroyl group that become negative with the loss of one proton to the media.

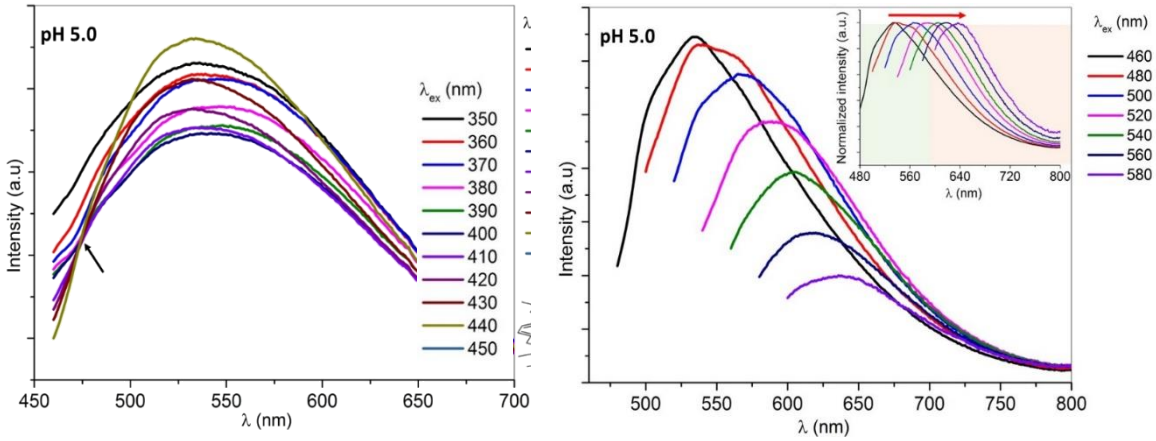

Figure 2 - Left: GQD-CB emission spectra at pH 5 for λex=350-450 nm (isobestic point, no redshift). Right: GQD-CB emission spectra at pH 5 for λex=460-580 nm (redshift).

When the samples were excited in the range of 350-450 nm, there was a crescent redshift on GQD's emission at pH above 8, corresponding to an increase of ionized groups. For instance, at pH 11.5, for λex=350-400 nm the GQD-CB presented blue emission whereas from λex=400-450 nm GQD-CB presented green emission. For all the pH values the maximum λex was 450 nm and for this wavelength GQD-CB presented green emission.
At pH 5, it was also possible to observe that, while at λex=350-450 nm there was no observable red shift, for higher excitation wavelengths (460-580 nm) a red shift occurred from a green emission at λex=450 nm to a red emission for λex=540-580 nm. GQD-CB fluorescence is therefore tunable with λex and pH.

The presence of two fluorescent species on GQD-CB resultant from the dissociation of carboxyl and hydroxyaroyl groups are confirmed by the zeta potential measurements, where it is possible to see three main regions: until pH 5 (GQD-CB almost neutral, ζ<-10mV, carboxyl and hydroxyaroyl protonated), between pH 5 and 9 (GQD-CB becoming negative, -10mV <ζ<-20mV, carboxyl group negative and hydroxyaroyl protonated), above pH 9 (GQD-CB becoming strongly negative, -20mV <ζ<-50mV, carboxyl and hydroxyaroyl groups negative) (Figure 3).

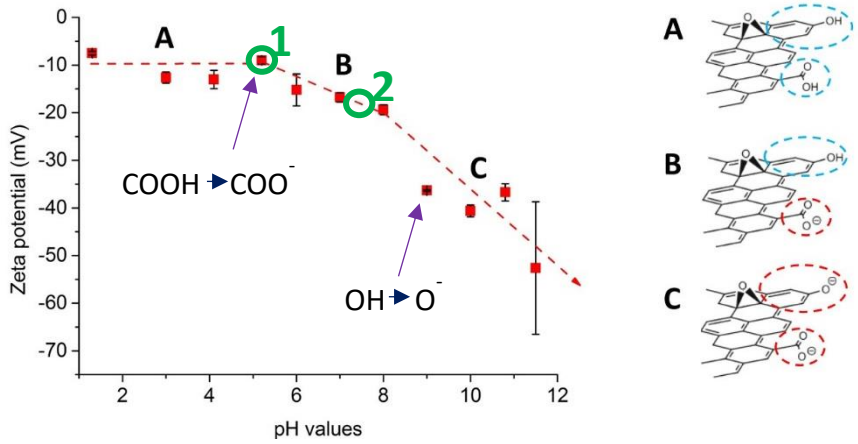

Figure 3 - Variation of zeta potential values (mV) of GQD-CB with pH. Regions A, B and C are defined according to the variation of zeta potential: (A) zeta-potential is almost constant; (B) zeta potential decreases, and (C) zeta-potential decreases more steeply. 1-cancer cells pH; 2-blood circulation pH. On the right: structural model of GQD-CB showing its probable edge groups ionization at each pH.

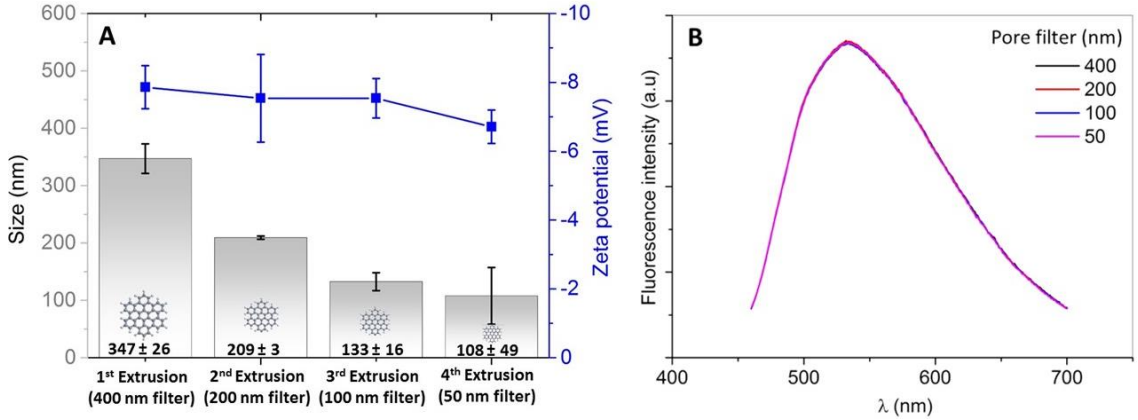

Figure 4 - (A) DLS and ELS characterization of GQDext. Size(nm) and zeta-potential (mV) measured for GQD-CBext obtained by extrusion, using consecutively filters of 400 nm, 200 nm 100 nm and 50 nm pores. Error bars correspond to STD of three measurements. (B) Fluorescence characterization of GQDext.

Spectroscopic methods of characterization indicate that GQD produced by chemical synthesis are randomly sized distributed. From the extrusion process it was possible to achieve a decrease on the size of GQD-CB maintaining both zeta potential and fluorescence properties as shown in

Figure 4. These results suggest that extrusion seems to be a promising process for size separation of GQD-CB.

The alternative process to produce GQD was CVD, but GQD-CVD were deposited into a glass substrate in a randomly sized distribution, as observed by confocal Raman and SEM. Therefore an extraction method was developed to extract GQD-CVD from glass substrate. Despite of the extraction method seemed to be promising, further studies should be performed.

3.2 DOX characterization

The *in silico* study of DOX showed a huge chemical complexity of this drug. However, it is possible to distinguish three main regions concerning DOX charge along pH: at pH = [0-8] DOX is positive due to NH_3^+, at pH = [8-9] DOX presents both positive (NH_3^+) and negative (O^-) charges and at pH>9 DOX is negatively charged due to the increasingly ionized O^- groups from quinone and anthraquinone and no positive charge (NH_3^+ become neutral NH_2) (Figure 5).

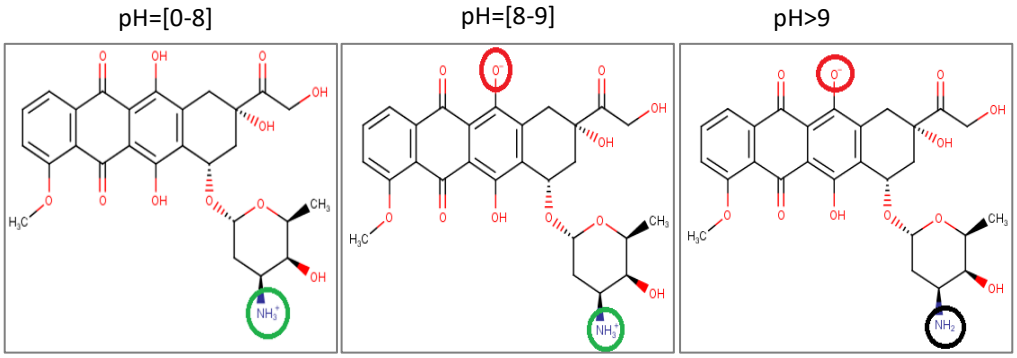

Figure 5 - Marvin Sketch® study of ionization of DOX reactive groups with pH.

DOX absorption maxima occur at λ = 233 nm, 253 nm, 290 nm, 481 nm, 495 nm and 530 nm. The UV spectra shows characteristic peaks of extended conjugation of an aromatic nucleus. The broad peak starting at 420 nm is indicative of the highly conjugated anthraquinone moiety. This gives the compound its red colour (Figure 37). On adding alkali (pH >9), the UV-Vis spectrum shifts towards longer wavelength due to the characteristic indicator-like properties of quinones. The colour change associated with this spectral shift is from orange-red to violet-blue (Figure 6).

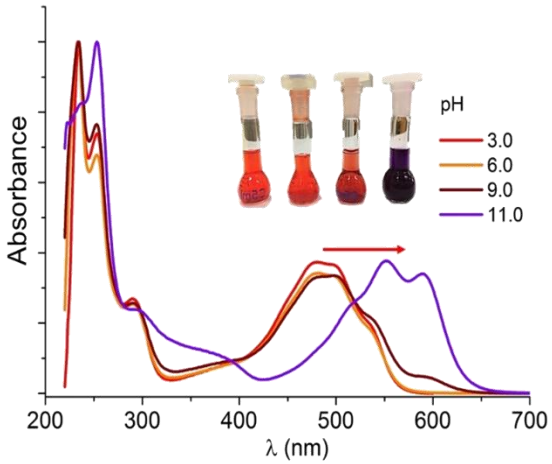

Figure 6 - DOX absorbance spectra at pH 3.0; 6.0; 9.0 and 11.0. Photo: DOX coloured solution at the mentioned pH values under visible light. Red arrow indicates spectra red shift with pH increase.

Given the absorbance dependence of DOX with the pH several DOX standards with rigorous concentrations were prepared in buffer at different pH values: 3.0, 4.7, 6.0, 9.0 and 11.0. The UV-VIS absorbance spectra of the DOX standards was measured and the Molar extinction coefficient or Molar absorptivity (ε in $Lmol^{-1}cm^{-1}$) was calculated (Figure 7). As it is possible to see on Table 1, ε decreases with increasing pH values. This means that for acidic pH there is no need for high concentrations to obtain high fluorescence, since the acid samples absorb more than the alkaline ones at the same concentration.

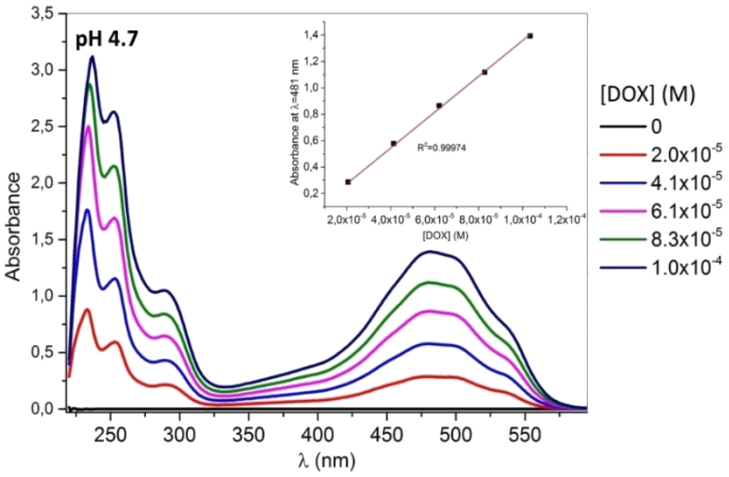

Figure 7 - DOX absorbance spectra of 5 standard solutions ($2x10^{-5}$ to $1x10^{-4}$ M) prepared in a buffered solution of pH 4.7. Inset: Beer Law linear plot for λ=481nm to obtain the molar absorptivity.

Table 1 - Molar absorptivity (ε in Lmol-1cm-1) and wavelengths where they were calculated for DOX at pH = 3.0, 4.7, 6.0, 9.0 and 11.0.

pH	ε_{DOX} ($Lmol^{-1}cm^{-1}$)	λ_{max} (nm)
3.0	10396	481
4.7	11450	482
6.0	10430	482
9.0	9426	498
11.0	7780	589

3.3 DOX-GQD-CB conjugates characterization

The *in silico* prediction (Figure 8) of interaction between DOX and GQD-CB indicates that in acid pH until 4.5-5.0, DOX is positively charged and GQD-CB are neutral, and thus an interaction between both is not expected. From pH 5.0 and 8.0, GQD-CB start to be more negative and DOX is still positive, promoting an adsorption between them. Within pH 8.0 and 9.0, GQD-CB increase their negative charge and DOX simultaneously has positive charges in $-NH_3^+$ group and $-O^-$ negative charges. Above pH 9, both DOX and GQD-CB are negatively charged through the deprotonation of OH groups and neutralization of $-NH_3^+$ group (DOX) and the appearance of more ionized edge groups, such as COO^- and Phe-O^- in the case of GQD-CB.

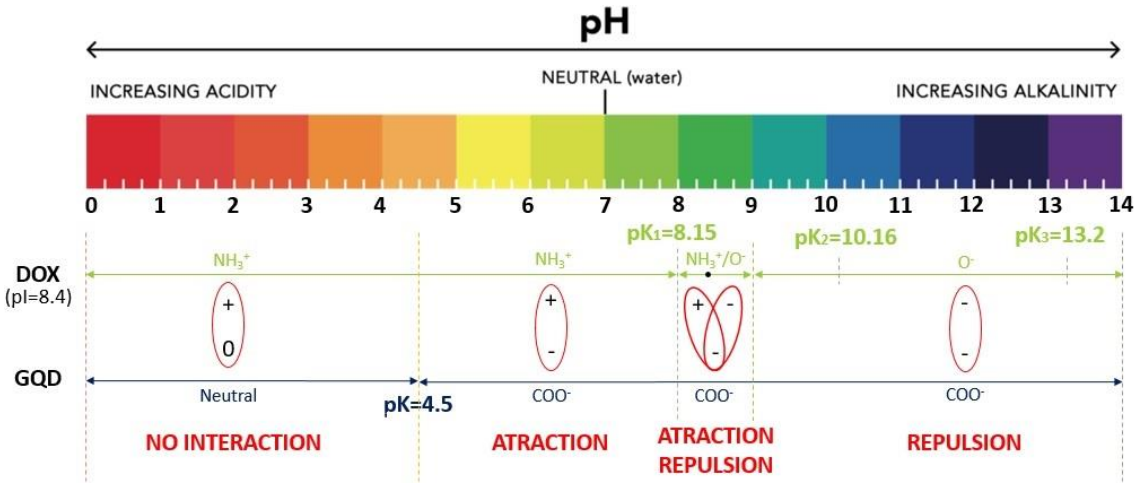

Figure 8 - Prediction of probable interaction between DOX and GQD-CB over pH variation.

As it is possible to observe in Figure 9, there was a total energy transfer from GQD-CB to DOX, for 450 nm excitation wavelengths at pH=6 (where is expected to be an attraction between DOX and GQD-CB). When GQD-CB and DOX are close located in the conjugate, the dots' emission energy was transferred to and absorbed by DOX and enhanced its final emission, as seen by the increase on the emitted fluorescence of the conjugates compared with DOX. This confirms the conjugates formation at pH=6.

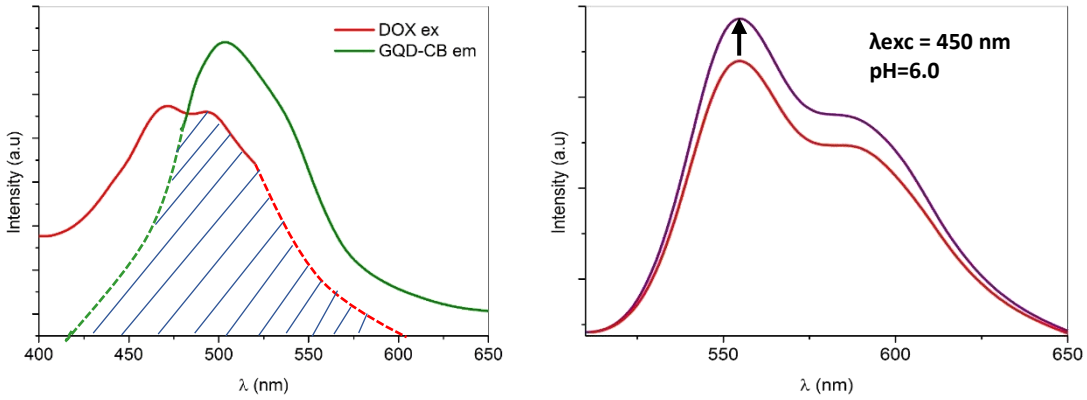

Figure 9 - Left: Fluorescence resonance energy transfer (FRET) of DOX-GQD-CB. Right: FL emission of DOX (red line) and DOX-GQD-CB (purple line) with the disappearance of GQD-CB emission.

The formation of DOX-GQD-CB conjugates at pH 6 was also confirmed by Raman and UV-VIS spectroscopy. ATR-FTIR analysis were not conclusive in this regard since DOX, GQD-CB and DOX-GQD-CB spectra were very similar.

From Raman analysis of GQD-CB at pH 6 it was possible to see both the G band (1590 cm^{-1}, in-plane vibration of sp2 bonded carbon) and the D band (1340 cm^{-1}, presence of sp3 defects in the termination plane of disordered carbons) (Figure 10A). This is in good agreement with the literature [13] [14] [15] [16]. Figure 10B shows the main DOX peaks, being the most intense band found at approximately 1412 cm^{-1} which may be attributed to the phenyl ring vibration, and it is also in agreement with what has been described in the literature [17].

On the DOX-GQD-CB spectrum (Figure 10C) there is the contribution of the main peaks of DOX and GQD-CB, with a lower I_D/I_G ratio, meaning less edge groups on the GQD-CB, which would be expected in the case of aggregation between DOX and GQD-CB. It was also visible a photothermic effect when increasing the laser intensity, disappearing the DOX peaks and decreasing more the I_D/I_G ratio, meaning that the dissociation of DOX from GQD-CB due to the laser intensity had probably reduced the edge groups from GQD-CB (Figure 10D).

From the UV-VIS spectroscopy it was possible to confirm the interaction prediction in Figure 8, since DOX-GQD-CB and DOX+GQD-CB spectra were not overlaid at pH 6 and 9 where it was expected to be an attraction between both, and it overlapped at pH 11 and 3 where it would be expected to be no interaction or repulsion. Also the visible peaks suffered a redshift with the increase of DOX concentration for the same concentration of GQD-CB at pH 6 and 9, and almost none for pH 3 and 11, meaning the concentration of DOX affected the formation of conjugates at pH 6 and 9 and do not for 3 and 11. (Figure 11)

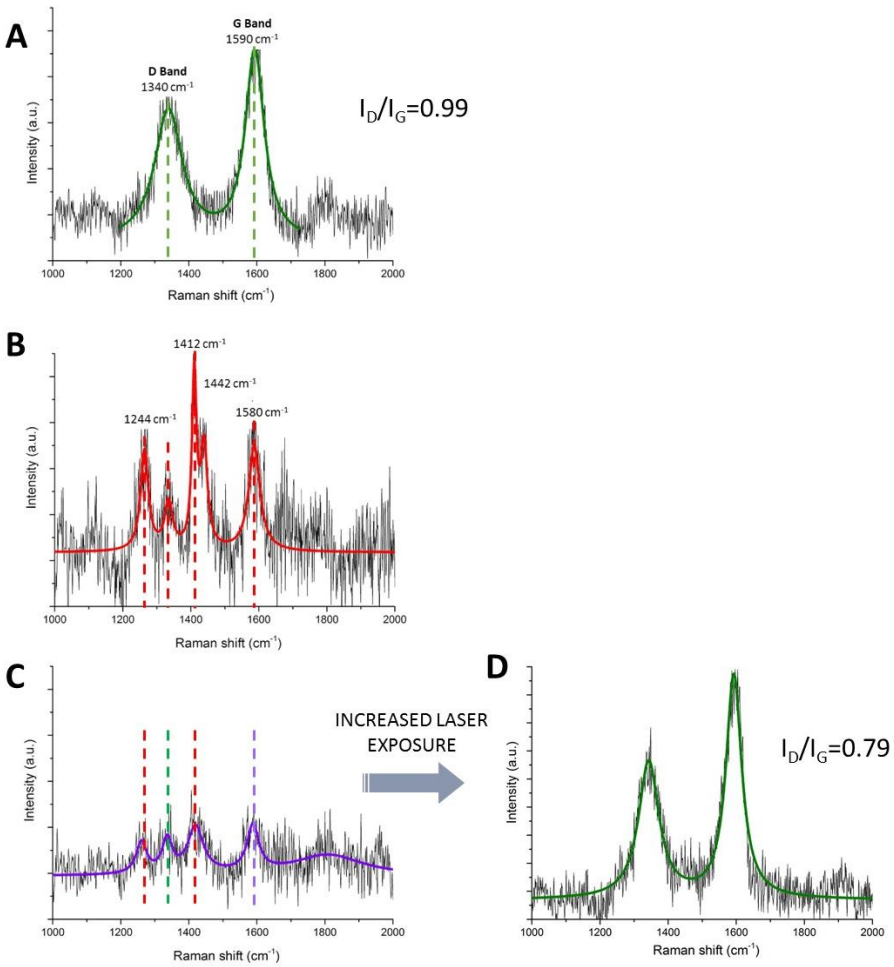

Figure 10 - Raman spectra of GQD-CB (A), DOX (B) and conjugates DOX-GQD-CB (C) at pH 6. (D) is the Raman spectrum obtained after exposing (C) to increased laser voltage. Peaks where fitted by Lorentzian function and fittings are displayed as green lines (A and D), red line (B) and violet line (C). In Figure C assignments of vibrational modes of DOX, GQD-CB or both are respectively identified by the red, green and violet dashed lines.

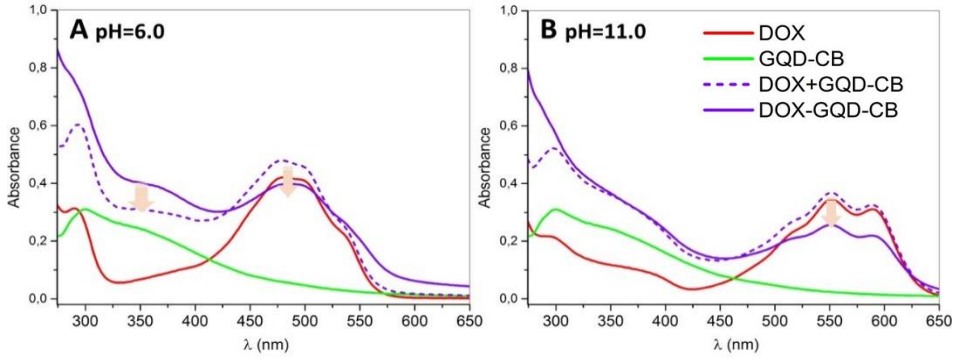

Figure 11 - Absorption spectra measured for free DOX, GQD-CB, DOX-GQD-CB (solid lines) and absorption spectra calculated by the sum of spectrum of DOX and GQD-CB (dashed lines) at pH 6.0 (A) and 11.0 (B) with a DOX concentration of $4.0x10^{-5}$ M.

3.4 GQD incorporation into liposomes

The comparison of the quenching effect of the different GQD incorporated in the lipid membranes is shown in **Erro! A origem da referência não foi encontrada.** for both 3AS and 12AS probes.

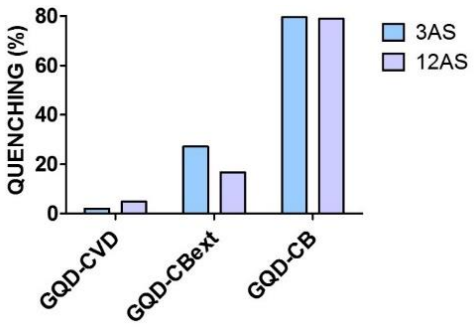

Figure 12 - Quenching of fluorescence emission (%) of the probes 3AS and 12AS (λex=360 nm) induced by the incorporation of GQD-CVD, GQD-CB and GQD-CBext in labelled lipid membranes.

To sum up, GQD-CVD were not very effective quenching the fluorescence of the probes, meaning that the graphene dots were too big to penetrate into the membrane, or that the extraction procedure was not effective to remove high concentration of GQD-CVD from the substrate. Unprocessed GQD-CB were the most effective quenching both probes with no apparent distinction meaning that they are able to penetrate the lipid membranes. Extruded GQD-CBext had a visible quenching effect and apparently with higher effect at the membrane headgroup regions.

4. Conclusions

At the end of this study promising methods of preparation and separation of GQD-CB by size extrusion were achieved. Furthermore, the negative ionization of GQD-CB and positive ionization of DOX at blood circulation pH (7.4) promote their attraction and adsorption, being the GQD-CB good to be used as nanocarriers and photosensitive agents. The neutral charge of GQD-CB and positive ionization of DOX at cancer cells pH (≈5) promote their desorption in that medium, allowing to conclude that the self-triggering at cancer cells can be achieved with DOX-GQD-CB conjugates. As future work we propose to study DOX controlled release mechanism by titration of conjugates. Furthermore, the encapsulation of conjugates into liposomes should also be studied, as well as the targeting and stealthy strategies. Finally, it would be essential to study the LNC formation in cancer cells *in vitro* and *in vivo*.

5. References

[1] Infarmed - National Version , "Doxorrubicina Medicamento," SPC (PT), Lisboa, 2014.

[2] M. Lúcio, "GraphLightCancer Graphene Quantum Dots for a Theranostic Approach to Cancer Treatment," Universidade do Minho, Braga, Portugal, 2016.

[3] PubChem - Open Chemistry Database, "Compound Summary for CID 31703 Doxorubicin," [Online]. Available: https://pubchem.ncbi.nlm.nih.gov/compound/doxorubicin. [Acedido em 05 2016].

[4] DrugBank, Canada, "DrugBank Drugs," DrugBank, [Online]. Available: https://www.drugbank.ca/drugs/DB00997. [Acedido em 06 2016].

[5] Y. (. Barenholz, "Doxil® — The first FDA-approved nano-drug: Lessons learned," *Journal of Controlled Release,* vol. 160, pp. 117-134, 2012.

[6] R. Anand, S. Ottani, F. Manoli, I. Manet e S. Monti, "A close-up on doxorubicin binding to c-cyclodextrin: an elucidating spectroscopic, photophysical and conformational study," *RSC Advances,* vol. 2, pp. 2346-2357, 2012.

[7] G. Raval, "Thermodynamic and Spectroscopic Studies on the Molecular Interaction of Doxorubicin (DOX) with negatively charged Polymeric Nanoparticles," Department of Pharmaceutical Sciences, University of Toronto, Canada, 2012.

[8] P. Yousefpour, F. Atyabi, E. V. Farahani, R. Sakhtianchi e R. Dinarvand, "Polyanionic carbohydrate doxorubicin–dextran nanocomplex as a delivery system for anticancer drugs: in vitro analysis and evaluations," *International Journal of Nanomedicine,* vol. 6, pp. 1487-1496, 2011.

[9] N. Yabbarov, G. Posypanova, E. Vorontsov, O. Popova e E. S. Severin, “Targeted Delivery of Doxorubicin: Drug Delivery System Based on PAMAM Dendrimers,” *Biochemistry,* Vols. %1 de %278, No.8, pp. 884-894, 2013.

[10] P. Changenet-Barret, T. Gustavsson, D. Markovitsi, I. Manet e S. Monti, “Unravelling molecular mechanisms in the fluorescence spectra of doxorubicin in aqueous solution by femtosecond fluorescence spectroscopy,” *Phys.Chem. Chem. Phys.,* vol. 15, pp. 2937-2944, 2013.

[11] R. J. Sturgeon e S. G. Schulman, “Electronic Absorption Spectra and Protolytic Equilibria of Doxorubicin: Direct Spectrophotometric Determination of Microconstants,” *Journal of Pharmaceutical Sciences,* Vols. %1 de %266, No.7, pp. 958-961, July 1977.

[12] N. Raghunand, X. He, R. v. Sluis, B. Mahoney, B. Baggett, C. Taylor, G. Paine-Murrieta, D. Roe, Z. Bhujwalla e R. Gillies, “Enhancement of chemotherapy by manipulation of tumour pH,” *British Journal of Cancer,* vol. 80(7), pp. 1005-1011, 1999.

[13] Y. Qin, Z.-W. Zhou, S.-T. Pan, Z.-X. He, X. Zhang, J.-X. Qiu, W. Duan, T. Yang e S.-F. Zhou, “Graphene quantum dots induce apoptosis, autophagy, and inflammatory response via p38 mitogen-activated protein kinase and nuclear factor-kB mediated signaling pathways in activated THP-1 macrophages,” *Toxicology,* vol. 327, pp. 62-76, 2015.

[14] N. Suzuki, Y. Wang, P. Elvati, Z.-b. Qu, K. Kim, S. Jiang, E. Baumeister, J. Lee, B. Yeom, J. H. Bahng, J. Lee, A. Violi e N. A. Kotov, “Chiral Graphene Quantum Dots,” *ACS Nano,* pp. 1-38, 2016.

[15] S. Kochmann, T. Hirsch e O. S. Wolfbeis, “The pH Dependence of the Total Fluorescence of Graphite Oxide,” © Springer Science+Business Media, Germany, 2011.

[16] D. Pan, J. Zhang, Z. Li e M. Wu, “Hydrothermal Route for Cutting Graphene Sheets into Blue-Luminescent Graphene Quantum Dots,” *Advanced Materials,* vol. 22, pp. 734-738, 2010.

[17] G. DAS, A. NICASTRI, M. L. COLUCCIO, F. GENTILE, P. CANDELORO, G. COJOC, C. LIBERALE, F. D. ANGELIS e E. D. FABRIZIO, “FT-IR, Raman, RRS Measurements and DFT Calculation for Doxorubicin,” MICROSCOPY RESEARCH AND TECHNIQUE, Italy, 2010.

[18] Y. (. Barenholz, “Doxil® — The first FDA-approved nano-drug: Lessons learned,” 2012.

[19] R. Anand, S. Ottani, F. Manoli, I. Manet e S. Monti, “A close-up on doxorubicin binding to c-cyclodextrin: an elucidating spectroscopic, photophysical and conformational study,” 2012.

[20] P. Yousefpour, F. Atyabi, E. V. Farahani, R. Sakhtianchi e R. Dinarvand, “Polyanionic carbohydrate doxorubicin–dextran nanocomplex as a delivery system for anticancer drugs: in vitro analysis and evaluations,” 2011.

[21] N. Yabbarov, G. Posypanova, E. Vorontsov, O. Popova e E. S. Severin, “Targeted Delivery of Doxorubicin: Drug Delivery System Based on PAMAM Dendrimers,” Pleiades Publishing, Ltd., Moscow, 2013.

[22] P. Changenet-Barret, T. Gustavsson, D. Markovitsi, I. Manet e S. Monti, “Unravelling molecular mechanisms in the fluorescence spectra of doxorubicin in aqueous solution by femtosecond fluorescence spectroscopy,” 2013.

[23] R. J. Sturgeon e S. G. Schulman, “Electronic Absorption Spectra and Protolytic Equilibria of Doxorubicin: Direct Spectrophotometric Determination of Microconstants,” 1977.

[24] N. Raghunand, X. He, R. v. Sluis, B. Mahoney, B. Baggett, C. Taylor, G. Paine-Murrieta, D. Roe, Z. Bhujwalla e R. Gillies, “Enhancement of chemotherapy by manipulation of tumour pH,” 1999.

[25] M. Lúcio, C. Nunes, D. Gaspar, K. Gołe˛bska, M. Wisniewski, J. Lima, G. Brezesinski e S. Reis, “Effect of anti-inflammatory drugs in phosphatidylcholine membranes: A fluorescence and calorimetric study,” Elsevier, Portugal, Germany, 2008.

[26] Y. Qin, Z.-W. Zhou, S.-T. Pan, Z.-X. He, X. Zhang, J.-X. Qiu, W. Duan, T. Yang e S.-F. Zhou, “Graphene quantum dots induce apoptosis, autophagy, and inflammatory response via p38 mitogen-activated protein kinase and nuclear factor-kB mediated signaling pathways in activated THP-1 macrophages,” 2015.

[27] N. Suzuki, Y. Wang, P. Elvati, Z.-b. Qu, K. Kim, S. Jiang, E. Baumeister, J. Lee, B. Yeom, J. H. Bahng, J. Lee, A. Violi e N. A. Kotov, “Chiral Graphene Quantum Dots,” 2016.

[28] D. Pan, J. Zhang, Z. Li e M. Wu, “Hydrothermal Route for Cutting Graphene Sheets into Blue-Luminescent Graphene Quantum Dots,” Advanced Materials, China, 2010.